PCCP

PAPER

View Article Online
View Journal | View Issue

Cite this: *Phys. Chem. Chem. Phys.*, 2015, **17**, 4569

Mutual solubilities between water and non-aromatic sulfonium-, ammonium- and phosphonium-hydrophobic ionic liquids†

Kiki A. Kurnia,[a] Maria V. Quental,[a] Luís M. N. B. F. Santos,[b] Mara G. Freire*[a] and João A. P. Coutinho[a]

Received 17th November 2014,
Accepted 2nd January 2015

DOI: 10.1039/c4cp05339g

www.rsc.org/pccp

Although previous studies attempted to characterize the liquid–liquid phase behaviour between water and ionic liquids (ILs), the impact of non-cyclic cations on the solubilities is poorly studied and yet to be understood. In this work, the mutual solubilities between water and ILs containing the anion bis(trifluoromethylsulfonyl)imide, $[NTf_2]^-$, combined with the cations diethylmethylsulfonium, $[S_{221}][NTf_2]$, triethylsulfonium, $[S_{222}][NTf_2]$, butyltrimethylammonium, $[N_{4111}][NTf_2]$, tributylmethylammonium, $[N_{4441}][NTf_2]$, methyltrioctylammonium, $[N_{1888}][NTf_2]$, and methyltrioctylphosphonium, $[P_{1888}][NTf_2]$, from (288.15 to 318.15) K and at 0.1 MPa, were experimentally measured and further compared with predictions from the COnductor-like Screening MOdel for Real Solvents (COSMO-RS). All the studied phase diagrams display an upper critical solution temperature (UCST). The binary system composed of $[P_{1888}][NTf_2]$ exhibits the widest immiscibility gap, followed by $[N_{18888}][NTf_2]$, $[N_{4441}][NTf_2]$, $[S_{222}][NTf_2]$, $[N_{4111}][NTf_2]$, and $[S_{221}][NTf_2]$. The COSMO-RS is able to correctly predict the experimental UCST behaviour and the cation impact on the immiscibility regimes observed. Natural Population Analysis (NPA) calculations were additionally performed for the isolated cations in the gas phase indicating that the differences in the water–IL mutual miscibilities might not result only from the hydrophobicity of the cation (derived from the increase of the alkyl chains length) but also from the charge distribution of the central atom and attached methylene groups. This fact explains the enhanced solubility of ammonium-based ILs in water here identified.

Introduction

Ionic liquids (ILs) are salts composed of a poorly coordinating and bulky organic cation combined with an organic or inorganic anion, which lead to a low melting temperature.[1] The ionic nature of these fluids provides many unique and attractive physical and chemical characteristics favourable to numerous applications. The characteristics of most ionic liquids include high thermal stability, large liquidus temperature range, high ionic conductivity, negligible vapour pressure, non-flammability, and high solvating capacity for organic, inorganic, and organometallic compounds.[1] Many of these physical and chemical properties can be designed by appropriate selection of the cation and anion to exhibit a specific set of intrinsic properties for a particular application. The applications of ILs have been summarized in a number of excellent reviews.[2–6] With regard to their potential application in separation processes, there is considerable interest in replacing conventional volatile organic solvents with ILs. In particular, it has been reported that ILs have a high capacity for the separation of metal ions,[7,8] organic compounds,[9–11] and biofuels[12–14] from aqueous solution. For instance, for the latter application, Simoni *et al.*[13] have shown that hydrophobic ILs are capable of extracting 1-butanol from aqueous solutions with a selectivity up to 300-fold. Neves *et al.*[15] suggested that phosphonium-based ILs are also potential alternatives for the extraction of ethanol from fermentation broths. In this respect, mutual solubilities of ILs and water are essential for the design and development of separation processes and they are also important for the evaluation of their environmental impact. The critical aspect here is that some ILs are toxic, and if they are released, either intentionally after industrial waste processing or accidentally during a spill, they would likely enter the aquatic ecosystems. In conclusion, the knowledge of the mixing behaviour between

[a] *Departamento de Química, CICECO, Universidade de Aveiro, 3810-193 Aveiro, Portugal. E-mail: maragfreire@ua.pt; Fax: +351-234-370084; Tel: +351-234-401422*

[b] *Centro de Investigação em Química, Departamento de Química e Bioquímica, Faculdade de Ciências da Universidade do Porto, R. Campo Alegre 687, P-4169-007 Porto, Portugal*

† Electronic supplementary information (ESI) available: Experimental data of mutual solubility of ILs and water; fitted parameters from the correlation of the experimental data with eqn (1) and (2); atom coordinates, charges from NPA, and σ-moment calculated at the BP-TZVP level of theory for water and ion composing the studied ILs; sigma profile and potential of water. See DOI: 10.1039/c4cp05339g

ILs and water is of great relevance for their potential use in future chemical processes.

For the purpose of designing an IL for a given application, a strategy combining both experimental measurements and molecular modelling can improve our knowledge on essential features underlying thermodynamic phenomena, such as solubility behaviour and phase equilibrium. With this goal in mind, finding a relationship between the experimentally observed trends and the fundamental properties of the system, such as electronic and molecular structure, is useful for predicting the features of ILs and can be further used for choosing appropriate IL cation and anion combinations.[16] Molecular modelling approaches based on quantum chemical calculations, such as the COnductor-like Screening MOdel for Real Solvents (COSMO-RS),[17,18] which correlates with chemical engineering thermodynamics in its-RS extension, can be used for such a purpose. COSMO-RS has been widely used for predicting liquid–liquid equilibrium (LLE) of systems containing ILs.[19,20] Unlike conventional thermodynamic models, such as Non Random Two-Liquid (NRTL), Universal Quasi-Chemical (UNIQUAC), or even UNIQUAC Functional-Group Activity (UNIFAC) coefficient models that require experimental data to fit the model parameters, the strength of COSMO-RS lies in the fact that it is an "*a priori*" method that only needs the chemical structures of the species involved as input. Through COSMO-RS, the behaviour of a species and its affinity towards other compounds can be used to extract a wealth of information regarding their interactions – in this work these are the ions composing the ILs and water. In addition, Natural Population Analysis (NPA)[21] calculations can be used to get deeper insights into the relationship of the cation electronic structure and its affinity towards water molecules. The NPA calculations allow estimating the charge distribution of the cation atom core, as well as of the aliphatic tails surrounding the cation core, and its subsequent impact on the interactions of ILs with water.

This work addresses the study of the mutual solubilities between ILs and water attempting to relate them with the chemical structure of ILs.[22,23] The ultimate goal is to create general rules for the design of hydrophobic ILs for a given task. To this end, previous studies focused on the effect of several IL chemical structural characteristics through their phase behaviour with water, namely the IL anion nature,[24] the cation core,[24] the alkyl side chain length at the cation,[25,26] and the presence of structural/positional isomers.[27–29] All of these systems exhibited an upper critical solution temperature (UCST).[23–29] It has been shown than the IL anion has a more significant impact on their mutual solubilities with water.[24] Nevertheless, and albeit to a weaker extent, the cation head group and the alkyl chain length of the ILs can also be used to fine-tune their mutual solubilities with water.[24,25] Furthermore, it has been shown that the solubility of ILs (for similar anion-based ILs) in water is entropically driven and mainly depends on their molecular volume.[28,30] Subsequently, simple correlations between the mole fraction solubility of ILs in water and their molecular volume were recently proposed.[28,30] Moreover, aiming at predicting the mutual solubilities between ILs and water, a quantitative structure–property relationship (QSPR) was also suggested.[31] In order to extend these studies to other ILs with different chemical structures than those previously investigated, several non-aromatic and non-cyclic ILs, namely with sulfonium, ammonium, or phosphonium cations, combined with the bis(trifluoromethylsulfonyl)imide anion ($[NTf_2]^-$), were here studied through the determination of their mutual solubilities with water. The chemical structure of the ions composing the studied ILs is depicted in Fig. 1. To the best of our knowledge there are only few reports providing the mutual solubilities of non-aromatic and non-cyclic ammonium-based[32] or phosphonium-based[33] ILs with water, and mutual solubilities between water and sulfonium-based ILs are here reported for the first time. From the obtained temperature-dependence solubility data, the thermodynamic properties of a solution of diethylmethylsulfonium bis(trifluoromethylsulfonyl)imide ($[S_{221}][NTf_2]$), triethylsulfonium bis(trifluoromethylsulfonyl)imide, ($[S_{222}][NTf_2]$), butyltrimethylammonium bis(trifluoromethylsulfonyl)imide ($[N_{4111}][NTf_2]$), and tributylmethylammonium bis(trifluoromethylsulfonyl)imide ($[N_{4441}][NTf_2]$) in water (at the water-rich phase) and of water in methyltrioctylammonium bis(trifluoromethylsulfonyl)imide ($[N_{1888}][NTf_2]$) and methyltrioctylphosphonium, bis(trifluoromethylsulfonyl)imide ($[P_{1888}][NTf_2]$) (at the IL-rich phase) were also derived and discussed. In addition, two different computational approaches, namely COSMO-RS and NPA calculations, were performed aiming at gathering a broader picture behind the IL–water interactions which dominate the liquid–liquid phase behaviour.

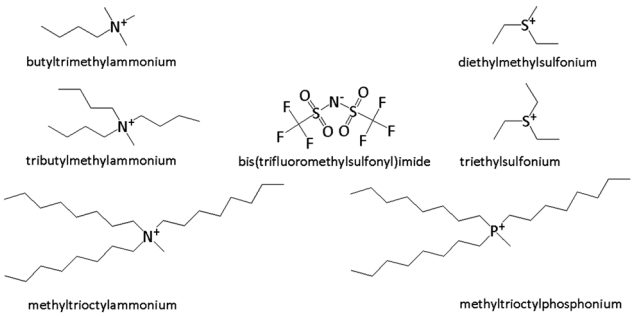

Fig. 1 Chemical structures of the ions composing the ILs studied in this work.

Results and discussion

The mutual solubilities between the studied non-cyclic ILs and water were measured within the temperature range from (288.15 to 318.5) K and at atmospheric pressure. The novel experimental solubility data and the respective standard deviations are depicted in Fig. 2, and presented in Tables S1a and S2a in the ESI.† Due to the high hydrophobic nature of $[N_{1888}][NTf_2]$ and $[P_{1888}][NTf_2]$, the solubility of these ILs in water is very low and below the detection limit of the conductivity method; thus, only the water solubility in these ILs is reported.

The mole fraction solubility of water in ILs is in the order of 10^{-1} to 10^{-2} (depending on the IL cation). While the mole fraction solubility of water in $[S_{221}][NTf_2]$, $[S_{222}][NTf_2]$, $[N_{4111}][NTf_2]$ and $[N_{4441}][NTf_2]$ indicates that these ILs are considerably "hygroscopic", on the other hand, the solubility of water in $[N_{1888}][NTf_2]$

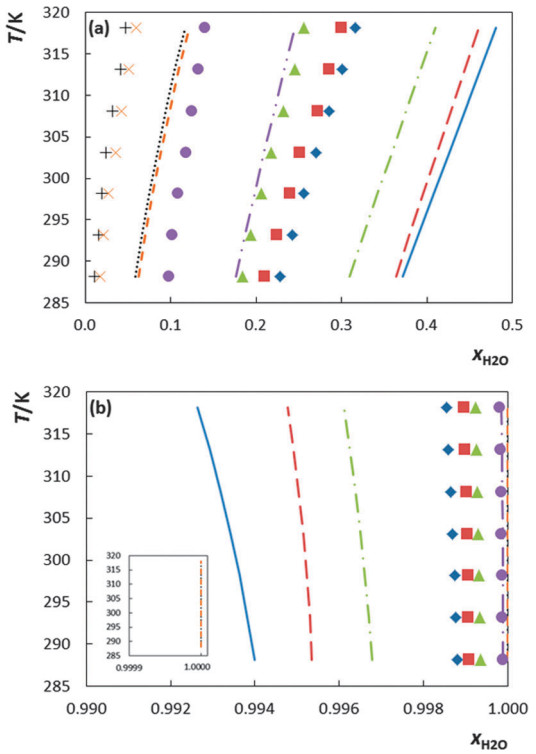

Fig. 2 Liquid–liquid phase diagrams for the binary mixtures composed of water and ILs: (a) IL-rich phase; and (b) water-rich phase. Symbols, lines: (♦, —), $[S_{221}][NTf_2]$; (■, —), $[N_{4111}][NTf_2]$; (▲, —·—), $[S_{222}][NTf_2]$; (●, —··—), $[N_{4441}][NTf_2]$; (×, ---), $[N_{1888}][NTf_2]$; and (+, ···), $[P_{1888}][NTf_2]$. The symbols and lines represent experimental and COSMO-RS prediction data, respectively. The inset represents the COSMO-RS predictions data for $[N_{1888}][NTf_2]$ and $[P_{1888}][NTf_2]$ solubilities in water.

and $[P_{1888}][NTf_2]$ is one order of magnitude lower and these IL-rich phases can be considered at infinite dilution. Furthermore, the mole fraction solubility of ILs in water ranges from 10^{-3} to 10^{-4} (and would be even lower for $[N_{8881}][NTf_2]$ and $[P_{8881}][NTf_2]$ that were not determined since their solubilities in water are below the detection limit of the equipment used). Therefore, the water-rich phase can be considered almost as a pure phase with the dissolved IL at infinite dilution. Nevertheless, it should be pointed out that due to large differences in the molecular weight between water and the studied ILs, when those values are converted to mass fraction compositions, the solubility of water in the IL is of the same order of magnitude to the solubility of the ILs in water (*cf.* Tables S1b and S2b in the ESI†).

The liquid–liquid phase diagrams of the investigated ILs, along with the respective COSMO-RS predictions, are depicted in Fig. 2. All the studied binary mixtures exhibit an upper critical solution temperature (UCST) behaviour, as previously reported for other ILs.[24–28] The most noticeable result is that the binary system composed of $[P_{1888}][NTf_2]$ exhibits the widest immiscibility gap, followed by $[N_{1888}][NTf_2]$, $[N_{4441}][NTf_2]$, $[S_{222}][NTf_2]$, $[N_{4111}][NTf_2]$ and $[S_{221}][NTf_2]$. In general, and comparing ILs with the same central atom, the mutual solubilities decrease from $[S_{221}][NTf_2]$ to $[S_{222}][NTf_2]$, and from $[N_{4111}][NTf_2]$ to $[N_{4441}][NTf_2]$ to $[N_{8881}][NTf_2]$. This is a well-established trend[25] by which an increase in the size of the aliphatic moieties attached to the cation core leads to an increase in the IL hydrophobicity, and therefore to a decrease in their mutual miscibilities with water, thus showing that the cation also has an influence and can be used to further tune this property. Moreover, phosphonium-based ILs are more hydrophobic than their ammonium-based counterparts, *i.e.*, $[P_{1888}][NTf_2]$ exhibits a lower solubility of water (at the same temperature) than $[N_{1888}][NTf_2]$. Although no data could be measured for the other side of the phase diagram, this trend is supported by previous results showing the higher hydrophobicity of phosphonium-based ILs.[22]

It is interesting to highlight that the binary mixtures composed of $[S_{222}][NTf_2]$ exhibit a wider immiscibility gap when compared to $[N_{4111}][NTf_2]$, despite the fact that the former has a lower number of total carbon atoms (or methylene groups) at the cation ($[S_{222}]^+$ = 6 carbon atoms and $[N_{4111}]^+$ = 7 carbon atoms). This is a clear indication that the mutual solubilities between water and ILs are not only related with the increase in the hydrophobic character of the cation derived from the increase of the alkyl chains, but are also governed by other factors, such as the charge distribution of the central atom and consequent charge distribution at the aliphatic moieties and further accessibility of water to the charged part of the cation.

COSMO-RS, partial charge and charge distribution

Prompted by the experimental results previously discussed, we turned our attention to the use of COSMO-RS and NPA calculations to get a deeper insight into the molecular mechanisms (or dominant interactions) which rule the liquid–liquid phase behaviour between the studied non-cyclic ILs and water. As a first approach, the ability of COSMO-RS to predict the LLE between ILs and water was evaluated. As depicted in Fig. 2, it is noticeable that the COSMO-RS model overestimates the mole fraction solubility of water in the studied ILs and *vice versa*. This might be related with the overestimated values of hydrogen-bonding energies between water and the studied ILs.[34] Some improvements can therefore be made (to achieve a better description of the mutual solubilities between water and ILs), such as by changing the IL–water hydrogen-bonding energies.[35] Nevertheless, it should be highlighted that the COSMO-RS model is able to correctly predict the UCST behaviour as well as the IL sequence experimentally observed. Moreover, COSMO-RS is also able to predict the very low solubility of $[N_{1888}][NTf_2]$ and $[P_{1888}][NTf_2]$ in water, to be in the order of 10^{-7} in mole fraction (*cf.* inset in Fig. 2b), and which are below the detection limit of the conductivity-based methodology used in this work. In this context, COSMO-RS can be used as a valuable tool to further characterize the water–IL main interactions.

COSMO-RS

COSMO-RS can be used to study the behaviour of individual components in a given mixture and their affinity towards another component in terms of sigma profiles and potentials, respectively. The detailed description of the meaning of sigma-profiles and potentials is given in the original work of Klamt.[18] The key feature of the sigma-profile is that when the screening charge density goes beyond ± 1.0 e nm^{-2}, the molecule is polar

enough to form hydrogen-bonds. The higher the absolute value of the charge density is, the stronger the compound is as a HB acceptor (+) or HB donor (−). Quantitatively, there are two important σ-moments related to hydrogen-bonding, namely HB_acc3 and HB_don3, which represent, respectively, the capability of individual atoms in the molecule to act as hydrogen bond acceptors and donors.[18,36] The σ-moments of water and of the ions composing the studied non-cyclic ILs are given in Tables S3–S10 in the ESI.†

The sigma profile of water (*cf.* Fig. S1a in the ESI†) ranges from −2.0 to 2.2 e nm^{-2}, and well beyond the ±1.0 e nm^{-2} cut off. This pattern indicates a high polarity of the molecule and its strong ability to form hydrogen bonds. The peak within the negative region, at 1.8 e nm^{-2}, is assigned to the oxygen atom that can act as a HB acceptor (HB_acc3 H_2O = 5.6933). On the other hand, the hydrogen atom exhibits a peak within the positive region, at −1.6 e nm^{-2}, confirming its capability as a HB donor (HB_don3 H_2O = 3.8506). These values reveal that water exhibits a strong ability to act either as a HB acceptor or as a HB donor, although being a stronger HB acceptor.

Fig. 3 depicts the sigma profiles and sigma potentials of the ions composing the studied ILs. The sigma profiles of all ions range within a narrower region when compared to that of water. The ions also exhibit significant peaks within the non-polar region, meaning that all ions have a non-polar character when compared with water. Furthermore, splitting the sigma-profiles of the studied ILs into their respective cation and anion allows us to study their individual effects and main interactions with water. For instance, the sigma profile of $[NTf_2]^-$ ranges from −0.4 e nm^{-2} (non-polar region) to 1.5 e nm^{-2} (H-bond acceptor region). The peak beyond the 1.0 e nm^{-2} cut off is observed at 1.1 e nm^{-2} (HB_acc3 $[NTf_2]^-$ = 2.2922). It is interesting to note that this anion only possesses HB-acceptor values whereas the cations retain the HB-donor ability (*cf.* Fig. 3). This indicates that the studied IL cations only act as H-bond donors while the anion only acts as a H-bond acceptor. By studying a set of ILs with the same anion, herein we force the condition that the differences in the mutual solubilities between water and ILs can only arise from the cation composing a given IL. With respect to the potential H-bond donor ability of the IL cation, this mainly arises from the hydrogen alpha, H_α (the hydrogen atom attached to the methylene groups more close to the central atom). This pattern suggests that the interactions between water molecules and the IL cation take place around H_α.

The sigma profiles of the IL cations, shown in Fig. 3, range between −1.5 e nm^{-2} (H-bond donor region) and 0.6 e nm^{-2} (non-polar region) with a peak (or shoulder-like peak) below the −1.0 e nm^{-2} cut-off, indicating therefore their subtle ability to act as HB donors. It should be highlighted that although the sigma profiles could be used to gather more insights into the behaviour of pure compounds (in this work, water and ILs) it does not take into account the interaction strength of the binary pairs. Thus, in this situation, other type of description, that is the sigma potential, is more important to describe the IL–water attraction. For example, and remarkably, the trend observed for the sigma-potentials of all the investigated ILs (right-side of Fig. 3b) clearly correlates with the IL–water mutual solubilities sequence (where the miscibility gaps decrease in the following order: $[P_{1888}][NTf_2]$ > $[N_{1888}][NTf_2]$ > $[N_{4441}][NTf_2]$ > $[S_{222}][NTf_2]$ > $[N_{4111}][NTf_2]$ > $[S_{221}][NTf_2]$). Furthermore, from the partial molar excess enthalpy, it can be seen that the dominant interaction in IL–water mixtures is hydrogen-bonding (*cf.* Table S11 in the ESI†). The electrostatic-misfit interactions and van der Waals forces have a weak contribution to the partial molar excess enthalpy of these mixtures.

Albeit the remaining ILs follow an expectable phase behaviour with water, the fact that $[N_{4111}][NTf_2]$, with a higher number of carbon atoms than $[S_{222}][NTf_2]$, exhibits a higher solubility in water needs further clarification. As previously mentioned, the immiscibility gap is related not only with the hydrophobicity of the IL derived from the size of the aliphatic moieties, but it is also governed by other factors, namely the charge distribution of the cation central atom and further ability of the IL cation for hydrogen-bonding with water.

Based on an analysis of COSMO-RS sigma profiles both $[S_{222}]^+$ and $[N_{4111}]^+$ exhibit a peak at −0.9 e nm^{-2}, with the latter having a higher intensity and containing a higher number of total carbon atoms at the aliphatic moieties. This translates into a

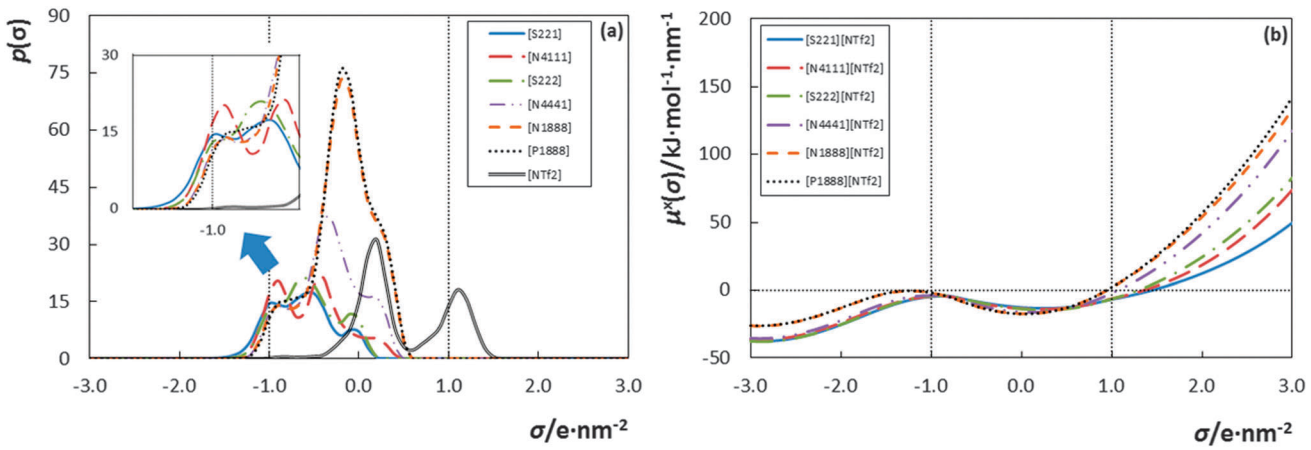

Fig. 3 Sigma-profiles (a) and sigma-potentials (b) of the ions composing the studied non-cyclic ILs computed by COSMO-RS.

higher affinity of $[N_{4111}][NTf_2]$ (HB_don3 = 0.2385) towards hydrogen bond acceptors, as depicted in Fig. 3b, when compared to $[S_{222}][NTf_2]$ (HB_don3 = 0.1868). Consequently, higher mutual solubilities between water and $[N_{4111}][NTf_2]$ are to be expected when compared to $[S_{222}][NTf_2]$, and are experimentally confirmed. Therefore, besides the IL hydrophobicity afforded by the size of the aliphatic tails, the hydrogen-bonding ability of the IL cation towards water molecules also seems to play an important role in their liquid–liquid phase behaviour.

To attempt to bring more support to this hypothesis we calculated the NPA charge distributions for the isolated ions in the gas phase. The coordinates and NPA charges for all atoms are given in the ESI.† It should be mentioned that the charge distribution in the isolated cations $[N_{1888}]^+$ and $[P_{1888}]^+$ is qualitatively comparable to those of the ion pairs $[N_{1888}][NTf_2]$ and $[P_{1888}][NTf_2]$, respectively.[37] Thus, it can be concluded that the NPA analysis of all isolated ions studied in this work is comparable with their respective cation–anion pairs.

NPA calculations of isolated $[S_{222}]^+$ and $[N_{4111}]^+$ cations yielded point-charge distributions showing that the hydrogen atoms are more positive while the carbon atoms are less negatively charged at the ammonium cation. The charges calculated for the central atoms are significantly different, namely +0.861 for S and −0.295 for N. Nevertheless, the hydrogens alpha, H_α, that are the hydrogens of the methylene group ($-CH_3$) directly connected to N are, in all cases, more positively charged than in the case of H_α of $-CH_2$ connected to S. Counting together the charge of the central atom and the charges of the adjacent alpha carbon and hydrogen, C_α and H_α, one reaches a slightly different net charge of the cationic centre: +0.831 for S and +0.929 for N. These results confirm that the positive charge is more distributed in $[N_{4111}]^+$ than in $[S_{222}]^+$ where it is mostly located at the central atom. They suggest that, while the S atom in $[S_{222}]^+$ is more charged than N in $[N_{4111}]^+$, the charge distribution of the latter makes the central part of the cation more charged, and thus more polar and with a higher affinity for water (as experimentally observed since $[N_{4111}][NTf_2]$ exhibits higher mutual solubilities with water than $[S_{222}][NTf_2]$). This charge distribution/contribution and further hydrogen-bonding ability is more important in the water solubility in the IL-rich phase, more dominated by the solute–solvent interactions.

The higher water solubilities in $[N_{1888}][NTf_2]$ when compared to $[P_{1888}][NTf_2]$ can also be explained in the light of charge distribution of the corresponding central atom at the cation. The calculated charges at the core atom are significantly different: −0.288 (N) and +1.689 (P). Yet, when considering the centre charge and the charges of C_α and H_α, $[N_{1888}]^+$ exhibits a higher positive charge distribution, +0.810, when compared to +0.789 of $[P_{1888}]^+$. COSMO-RS also shows that $[N_{8881}][NTf_2]$ has a stronger H-bond donor ability than $[P_{8881}][NTf_2]$. Thus, for two cations with similar hydrophobicity, *i.e.* similar number and sizes of aliphatic tails, the following rule-of-thumb can be applied: the more positive the charge of the central part of the cation, the more intense the interaction between the IL cation and water.

Temperature dependence of the water solubility in ILs

Assuming that in the temperature range investigated the change in the standard molar enthalpy of solution of water in the IL phase is negligible, the temperature dependence of water solubility in ILs can be correlated using eqn (1), while the solubility of ILs in the water-rich phase can be correlated using eqn (2),

$$\ln x_w = A + \frac{B}{T/K} \quad (1)$$

$$\ln x_{IL} = C + \frac{D}{T/K} + E\ln(T/K) \quad (2)$$

where T is the temperature, and A, B, C, D, and E are fitted parameters. Those parameters and their standard deviations are presented in Table S12 in the ESI.† The proposed correlation shows a relative average deviation from the experimental mole fraction data of 1.3% for both rich phases.

As previously mentioned, the solubility of ILs in water (ranging from 10^{-3} to 10^{-4} in mole fraction) can be considered at infinite dilution. On the other hand, the water solubility in the studied ILs ranges from 10^{-1} to 10^{-2} (*cf.* Tables S1 and S2 in the ESI†). While $[S_{221}][NTf_2]$, $[S_{222}][NTf_2]$, $[N_{4111}][NTf_2]$, and $[N_{4441}][NTf_2]$ are considered hygroscopic (with a mole fraction solubility of water in the order of 10^{-1}), the low mole fraction solubility in $[N_{1888}][NTf_2]$ and $[P_{1888}][NTf_2]$ (in the order of 10^{-2}) is low enough to be considered at infinite dilution. Thus, it allows us to determine the associated standard thermodynamic molar functions of a solution of water in $[N_{1888}][NTf_2]$ and $[P_{1888}][NTf_2]$, namely the standard molar Gibbs energy, $\Delta_{sol}G^0_m$, the enthalpy, $\Delta_{sol}H^0_m$, and entropy, $\Delta_{sol}S^0_m$, of solution, at 298.15 K, using eqn (3)–(5),

$$\Delta_{sol}G^0_m = RT\ln(x_1)_p \quad (3)$$

$$\frac{\Delta_{sol}H^0_m}{RT^2} = \left(\frac{\partial \ln x_1}{\partial T}\right)_p \quad (4)$$

$$\Delta_{sol}S^0_m = R\left[\frac{\partial(T\ln x_1)}{\partial T}\right]_p \quad (5)$$

where x_1 is the mole fraction solubility of water in IL, or IL in water, T is the temperature, R is the ideal gas constant, p = 0.1 MPa, and m refers to molar quantity. These thermodynamic properties, reported in Table 1, are associated with the changes that occur in the solute neighbourhood when one solute molecule is transferred from an ideal gas phase to a diluted ideal solution.

The high positive enthalpies of solution of water in $[N_{1888}][NTf_2]$ and $[P_{1888}][NTf_2]$ at 298.15 K indicate that the interaction between H_2O and these ILs is very weak due to the bulky alkyl chains in these ILs. Thus, the small solubility differentiation between the two ILs, $[N_{1888}][NTf_2]$ and $[P_{1888}][NTf_2]$, is ruled by the small differentiation in the enthalpy of solution that is higher (more positive) for $[P_{1888}][NTf_2]$ (IL with a lower solubility of water). The higher and almost not differentiated entropy of solution of water in both ILs reflects the entropy increment of water molecules in the IL solution when compared with water in the bulk phase.

Table 1 Thermodynamic standard molar properties of solution at 298.15 K along with the respective standard deviation, σ

IL	$(\Delta_{sol}H^0_m \pm \sigma)$/ (kJ mol^{-1})	$(\Delta_{sol}G^0_m \pm \sigma)$/ (kJ mol^{-1})	$(\Delta_{sol}S^0_m \pm \sigma)$/ (J K^{-1} mol^{-1})
Water in IL			
$[N_{1888}][NTf_2]$	32.5 ± 1.5	8.934 ± 0.003	79.0 ± 5.0
$[P_{1888}][NTf_2]$	33.6 ± 1.5	9.754 ± 0.006	80.6 ± 5.0
IL in water			
$[N_{4111}][NTf_2]$	2.4 ± 1.5	17.254 ± 0.006	−49.7 ± 5.0
$[N_{4441}][NTf_2]$	12.2 ± 1.5	22.006 ± 0.002	−32.8 ± 5.0
$[S_{221}][NTf_2]$	4.7 ± 1.5	16.539 ± 0.001	−39.8 ± 5.0
$[S_{222}][NTf_2]$	4.2 ± 1.5	18.088 ± 0.002	−46.5 ± 5.0

The enthalpies of solution of the ILs in water at 298.15 K are also positive, reflecting an endothermic process of dissolution, and are essentially very slightly dependent on the alkyl chain length, as typically observed with aromatic ILs.[24–28] However, it should be remarked that the $\Delta_{sol}H^0_m$ of $[N_{4441}][NTf_2]$ in water is significantly higher than those obtained for the remaining ILs. This unexpected behaviour might also be related with the distribution/contribution of the charges as previously discussed. The derived molar entropies of solution of ILs in water are negative, and reflect the high solvation entropic penalty of the water molecules to accommodate the IL ions or IL ion pairs. The entropic penalty in the ILs dissolution in water is the ruling factor for their low solubility – for the so-called hydrophobic ILs. The dissolution of the non-aromatic ILs in water is also entropically driven as previously shown for other families of ILs.[23–29] Interestingly, while a small decrease in the entropic effect of approximately −5 J K^{-1} mol^{-1} per methylene addition at the sulfonium cation is observed, and as previously shown for aromatic $[NTf_2]$-based ILs,[28] a decrease of only −3 J K^{-1} mol^{-1} for ammonium-based ILs is observed.

It is known that the solubility of poorly soluble organic compounds in water, including hydrophobic ILs composed of similar anions, is primarily dependent on their molar volume, V_m.[28] A correlation between the logarithm of the mole fraction solubility of ILs in water as a function of their molar volume, and previously proposed, is depicted in Fig. 4.[28] The V_m of each IL at 298.15 K was determined based on the experimental density data taken from the literature.[37–39] As shown in Fig. 4, the sulfonium-based ILs fall close to the correlation previously presented for a wide range of $[NTf_2]$-based ILs.[28] On the other hand, the ammonium-based ILs, and using data taken from this work and from the literature,[37–39] seem to be outsiders of this correlation. The differentiation in the ammonium-based IL behaviour, not previously reported, is a clear indication that the solubility of ammonium-based compounds, is not only governed by their molecular volume, as previously observed in similar ILs investigated,[28,29] but is also dependent on the particular cation charge distribution, as discussed before.

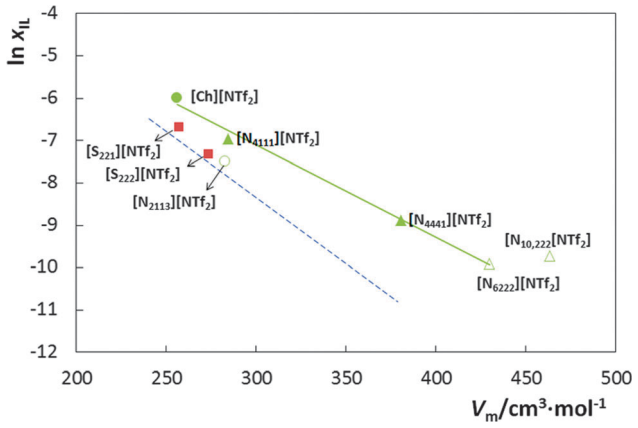

Fig. 4 Logarithm of solubility of $[NTf_2]$-based ILs in water (mole fraction) as a function of the molar volume of ILs. The symbol represents experimental data: (■), $[S_{221}][NTf_2]$ and $[S_{222}][NTf_2]$ (this work); (▲), $[N_{4111}][NTf_2]$ and $[N_{4441}][NTf_2]$ (this work); (△) $[N_{6222}][NTf_2]$ and $[N_{10,222}][NTf_2]$;[32,37] (●), $[N_{2113}][NTf_2]$;[39] (○), $[Ch][NTf_2]$.[39] The green line represents new correlation $\ln(x_{IL}) = -0.0218\ (V_m/cm^3\ mol^{-1}) - 0.5575$; $R^2 = 0.9930$. The dashed blue line represents the correlation for the ILs with the aromatic cation, previously reported. $\ln(x_{IL}) = -0.0309\ (V_m/cm^3\ mol^{-1}) + 0.9357$; $R^2 = 0.9947$.[28]

Conclusions

This work reports new experimental data and prediction results using COSMO-RS for the mutual solubilities between water and non-aromatic sulfonium-, ammonium-, or phosphonium-$[NTf_2]$-based ILs in the temperature range from 288.15 K to 318.15 K. In addition, NPA calculations were performed for the isolated cations in the gas phase to support the obtained experimental trends, as well as to gather a broader picture of the mechanisms ruling the IL–water phase behaviour. The main focus of this work was to analyse the impact of structural changes occurring on a non-cyclic cation, namely the number of alkyl chains and their length and cation central atom through the liquid–liquid phase behaviour with water. Experimental results and COSMO-RS predictions revealed the same trend of immiscibility gap for the studied non-cyclic ILs with water as well as their UCST behaviour. Furthermore, COSMO-RS and charge distribution calculations confirmed that the increase of the immiscibility gap of the studied non-cyclic ILs and water is not only caused by the hydrophobic character of the cation (derived from an increase in the alkyl side chains) but is also a result of the cation charge distribution. The charge distribution of the cation seems to play a considerable role in defining the mutual solubilities between water and $[S_{222}][NTf_2]$ *vs.* $[N_{4111}][NTf_2]$ and $[N_{1888}][NTf_2]$ *vs.* $[P_{1888}][NTf_2]$.

The standard molar thermodynamic functions of solution, at 298.15 K and infinite dilution, for water in $[N_{1888}][NTf_2]$ and $[P_{1888}][NTf_2]$, as well as for $[S_{221}][NTf_2]$, $[S_{222}][NTf_2]$, $[N_{4111}][NTf_2]$ and $[N_{4441}][NTf_2]$ in water, were determined. The results confirm that the dissolution of ILs in water is entropically driven. The small molar enthalpies of solution of water in $[N_{1888}][NTf_2]$ and $[P_{1888}][NTf_2]$ at 298.15 K support the weak IL–water interactions as a result of the bulky structure of these cations.

The results here reported, along with data for the solubility of other quaternary ammonium-based ILs previously reported in the literature, show that, unlike most $[NTf_2]$-based ionic liquids whose their solubility in water correlates with their molecular volume, for these compounds, the charge distribution of the

cation and further hydrogen-bonding ability also plays a significant role.

Experimental procedure

Chemicals

The experimental mutual solubilities with water were measured for the ILs composed of the bis(trifluoromethylsulfonyl)imide anion combined with the following cations: diethylmethylsulfonium, $[S_{221}][NTf_2]$ (99 wt%, Iolitec); triethylsulfonium, $[S_{222}][NTf_2]$ (99 wt%, Iolitec); butyltrimethylammonium, $[N_{4111}][NTf_2]$ (99 wt%, Iolitec); tributylmethylammonium, $[N_{4441}][NTf_2]$ (99 wt%, Iolitec); methyltrioctylammonium, $[N_{1888}][NTf_2]$ (99 wt%, Iolitec); and methyltrioctylphosphonium, $[P_{1888}][NTf_2]$ (98 wt%, Iolitec). The chemical structures of the studied compounds are presented in Fig. 1. To reduce the amounts of impurities that may be present, individual samples of ILs were dried under vacuum at 323.15 K and constantly stirred for a minimum period of 48 h. The purity of each IL was further checked by ^1H, ^{13}C and ^{19}F NMR. All samples exhibited purities according to those given by the manufacturers. The water content of the dried ILs was determined using a Metrohm 831 Karl Fischer (KF) coulometer, with the analyte Hydranal® – Coulomat AG from Riedel-de Haën, and was found to be below 100 ppm for all samples. Ultrapure water, double distilled, passed by a reverse osmosis system and further treated with a MilliQ plus 185 water purification apparatus, was used in the mutual solubility experiments. The water used exhibits a resistivity of 18.2 MΩ cm, a TOC smaller than 5 μg dm^{-3} and is free of particles >0.22 μm.

Apparatus and procedure

The mutual solubilities between water and ILs were determined in the temperature range from (288.15 to 318.15) K and at atmospheric pressure according to a method previously described.[28,30] The IL–water binary mixtures were put in tightly-closed glass vials with a septum cap. The samples were then vigorously stirred and allowed to settle and equilibrate inside an aluminum block, specially designed for this purpose, for at least 48 h. This period of time proved to be enough to guarantee a complete separation of the two phases, as well as their saturation.[24] The aluminium block is placed in an isolated air bath capable of maintaining the temperature within ±0.01 K. The temperature control was achieved using a PID temperature controller driven by a calibrated Pt100 (class 1/10) temperature sensor inserted in the aluminium block. A Julabo (model F25-HD) refrigerated bath and circulator was used as the cooling source of the thermostated aluminium block. Both phases were sampled at each temperature from the equilibrium vials using glass syringes maintained dry and kept at the same temperature of the measurements.

The solubility of water in the IL-rich phase was measured by KF titration. Approximately 0.1 g of the IL-rich phase was sampled and directly injected in the KF coulometric titrator to determine the water content (gravimetrically). The solubility of the studied ILs was determined by a conductivity method previously described.[30,31] The conductivity of the aqueous solution was measured using a Mettler Toledo S47 SevenMultiTM dual meter pH/conductivity, coupled with an inLab®741 Conductivity Probe as the electrode. In this method, approximately 0.5 g of the water-rich phase was sampled from the equilibrium glass vials and further diluted in ultra-pure water in a ratio of 1:20 (w:w). Previous optimization tests regarding the appropriate dilution were carried out aiming at obtaining significant conductivity values and within the equipment capability. Prior to the measurements, calibration curves were performed for each IL and in an adequate concentration range. Each stock solution was prepared gravimetrically within $\pm 10^{-5}$ g and at least 2 calibration curves were determined for each IL and to confirm that no gravimetric errors occurred during the preparation of each stock solution. Each measurement, at each temperature, was repeated at least 5 times, and the results are reported as the average solubility value along with the respective standard deviation.

COSMO-RS

COSMO-RS is a well-known predictive method developed by Klamt and co-workers for providing the thermodynamic equilibrium of fluids and mixtures by using a statistical thermodynamic approach based on previous results of unimolecular quantum chemical calculations.[17,18] The model can be used to predict the phase behaviour of binary mixtures and subsequently the concentration of each component in a given phase. Previously, we used COSMO-RS to predict the equilibrium behaviour of ILs and water and confirmed its high capability as a predictive tool.[28,30]

The standard procedure consists in two major steps: (i) the quantum chemical calculations to obtain the COSMO files and (ii) COSMO-RS calculations that use COSMO files as the only input and calculate the chemical potential and, thus, the liquid–liquid equilibrium between ILs and water. The quantum chemical COSMO calculations for the isolated cation, anion, and water molecules were performed at the density functional theory (DFT) level, utilizing the BP functional B88-P86 with resolution of identity approximation and triple-ζ valence polarized basis set (TZVP).[40–42] All calculations were performed using the TURBOMOLE 6.1 program package.[43] Vibrational frequency calculations to confirm the presence of an energy minimum in geometry optimizations were done to check the absence of negative values. After optimization, the generated cosmo files were then used to predict the equilibrium composition between ILs and water using the COSMOthermX program (Version C30 Release 13.01).[44] In all calculations, the ILs were always treated as isolated ions at the quantum chemical level. The detailed calculations of the phase equilibrium using COSMOthermX are explained in our previous work.[28] In addition, the best predictions of the experimental data were obtained with the lowest energy conformations or with the global minimum for both cation and anion.[45] Therefore, in this work, the lowest energy conformations of all the species involved were used in the COSMO-RS calculations.

Partial charge and charge distribution

The optimized geometries of isolated water, IL cation and anion obtained using TURBOMOLE 6.1 were used as the starting

structures and the full optimization was carried out using the TZVP basis set and the non-local BP exchange–correlation functional[40–42] as implemented in Gaussian 03 Revision D.02.[46] Thereafter, on the obtained minima, the partial charges and charges distribution of the isolated cation composing the studied non-cyclic ILs were retrieved by electrostatic surface potential (ESP) fits, using the NPA algorithm[21] to the electron densities obtained at the BP/TZVP level of theory.

Acknowledgements

This work was financed by national funding from Fundação para a Ciência e a Tecnologia (FCT, Portugal), European Union, QREN, FEDER and COMPETE for the projects PEST-C/CTM/LA0011/2013 and EXPL/QEQ-PRS/0224/2013. The authors also thank FCT for the postdoctoral grant SFRH/BPD/88101/2012 of K.A.K. M.G. Freire acknowledges the European Research Council (ERC) for the Grant ERC-2013-StG-337753.

Notes and references

1 P. Wasserscheid and T. Welton, *Ionic Liquids in Synthesis*, WILEY-VCH Verlag GmbH & Co. KGaA, Darmstadt, Federal Republic of Germany, 2nd edn, 2009, vol. 1.
2 T. Welton, *Chem. Rev.*, 1999, **99**, 2071.
3 V. I. Pârvulescu and C. Hardacre, *Chem. Rev.*, 2007, **107**, 2615.
4 J. Brennecke and E. J. Maginn, *AIChE J.*, 2001, **47**, 2384.
5 N. V. Plechkova and K. R. Seddon, *Chem. Soc. Rev.*, 2008, **37**, 123.
6 H. Passos, M. G. Freire and J. A. P. Coutinho, *Green Chem.*, 2014, **16**, 4786.
7 N. Papaiconomou, J.-M. Lee, J. Salminen, M. V. Stosch and J. M. Prausnitz, *Ind. Eng. Chem. Res.*, 2007, **47**, 5080.
8 N. Papaiconomou, S. Génand-Pinaz, J. M. Leveque and S. Guittonneau, *Dalton Trans.*, 2013, **42**, 1979.
9 S. Mohanty, T. Banerjee and K. Mohanty, *Ind. Eng. Chem. Res.*, 2010, **49**, 2916.
10 F. S. Oliveira, J. M. M. Araújo, R. Ferreira, L. P. N. Rebelo and I. M. Marrucho, *Sep. Purif. Technol.*, 2012, **85**, 137.
11 J. G. Huddleston and R. D. Rogers, *Chem. Commun.*, 1998, 1765.
12 A. Chapeaux, L. D. Simoni, T. S. Ronan, M. A. Stadtherr and J. F. Brennecke, *Green Chem.*, 2008, **10**, 1301.
13 L. D. Simoni, A. Chapeaux, J. F. Brennecke and M. A. Stadtherr, *Comput. Chem. Eng.*, 2010, **34**, 1406.
14 D. Rabari and T. Banerjee, *Fluid Phase Equilib.*, 2013, **355**, 26.
15 C. M. S. S. Neves, J. F. O. Granjo, M. G. Freire, A. Robertson, N. M. C. Oliveira and J. A. P. Coutinho, *Green Chem.*, 2011, **13**, 1517.
16 K. A. Kurnia, S. P. Pinho and J. A. P. Coutinho, *Green Chem.*, 2014, **16**, 3741.
17 A. Klamt and F. Eckert, *Fluid Phase Equilib.*, 2000, **172**, 43.
18 A. Klamt, *COSMO-RS from quantum chemistry to fluid phase thermodynamics and drug design*, Elsevier, Amsterdam, The Netherlands, 2005.
19 A. R. Ferreira, M. G. Freire, J. C. Ribeiro, F. M. Lopes, J. G. Crespo and J. A. P. Coutinho, *Ind. Eng. Chem. Res.*, 2011, **50**, 5279.
20 C. V. Manohar, D. Rabari, A. A. P. Kumar, T. Banerjee and K. Mohanty, *Fluid Phase Equilib.*, 2013, **360**, 392.
21 A. E. Reed, R. B. Weinstock and F. Weinhold, *J. Chem. Phys.*, 1985, **83**, 735.
22 P. J. Carvalho, S. P. M. Ventura, M. L. S. Batista, B. Schröder, F. Gonçalves, J. Esperança, F. Mutelet and J. A. P. Coutinho, *J. Chem. Phys.*, 2014, **140**, 064505.
23 K. A. Kurnia, T. E. Sintra, C. M. S. S. Neves, K. Shimizu, J. N. Canongia Lopes, F. Goncalves, S. P. M. Ventura, M. G. Freire, L. M. N. B. F. Santos and J. A. P. Coutinho, *Phys. Chem. Chem. Phys.*, 2014, **16**, 19952.
24 M. G. Freire, C. M. S. S. Neves, P. J. Carvalho, R. L. Gardas, A. M. Fernandes, I. M. Marrucho, L. M. N. B. F. Santos and J. A. P. Coutinho, *J. Phys. Chem. B*, 2007, **111**, 13082.
25 M. G. Freire, P. J. Carvalho, R. L. Gardas, I. M. Marrucho, L. M. N. B. F. Santos and J. A. P. Coutinho, *J. Phys. Chem. B*, 2008, **112**, 1604.
26 F. M. Maia, O. Rodríguez and E. A. Macedo, *Fluid Phase Equilib.*, 2010, **296**, 184.
27 M. G. Freire, C. M. S. S. Neves, K. Shimizu, C. E. S. Bernardes, I. M. Marrucho, J. A. P. Coutinho, J. N. Canongia Lopes and L. P. N. Rebelo, *J. Phys. Chem. B*, 2010, **114**, 15925.
28 M. A. R. Martins, C. M. S. S. Neves, K. A. Kurnia, L. Andreia, L. M. N. B. F. Santos, M. G. Freire, S. P. Pinho and J. A. P. Coutinho, *Fluid Phase Equilib.*, 2014, **375**, 161.
29 M. A. R. Martins, C. M. S. S. Neves, K. A. Kurnia, L. M. N. B. F. Santos, M. G. Freire, S. P. Pinho and J. A. P. Coutinho, *Fluid Phase Equilib.*, 2014, **381**, 28.
30 C. M. S. S. Neves, A. R. Rodrigues, K. A. Kurnia, J. M. S. S. Esperança, M. G. Freire and J. A. P. Coutinho, *Fluid Phase Equilib.*, 2013, **358**, 50.
31 M. G. Freire, C. M. S. S. Neves, S. P. M. Ventura, M. J. Pratas, I. M. Marrucho, J. Oliveira, J. A. P. Coutinho and A. M. Fernandes, *Fluid Phase Equilib.*, 2010, **294**, 234.
32 K. Machanová, J. Jacquemin, Z. Wagner and M. Bendová, *Procedia Eng.*, 2012, **42**, 1229.
33 M. G. Freire, P. J. Carvalho, R. L. Gardas, L. M. N. B. F. Santos, I. M. Marrucho and J. A. P. Coutinho, *J. Chem. Eng. Data*, 2008, **53**, 2378.
34 K. A. Kurnia and J. A. P. Coutinho, *Ind. Eng. Chem. Res.*, 2013, **52**, 13862.
35 C.-M. Hsieh, S. I. Sandler and S.-T. Lin, *Fluid Phase Equilib.*, 2010, **297**, 90.
36 T. Zhou, L. Chen, Y. Ye, Z. Qi, H. Freund and K. Sundmacher, *Ind. Eng. Chem. Res.*, 2012, **51**, 6256.
37 K. Machanová, A. Boisset, Z. Sedláková, M. Anouti, M. Bendová and J. Jacquemin, *J. Chem. Eng. Data*, 2012, **57**, 2227.
38 A. Bhattacharjee, A. Luís, J. H. Santos, J. A. Lopes-da-Silva, M. G. Freire, P. J. Carvalho and J. A. P. Coutinho, *Fluid Phase Equilib.*, 2014, **381**, 36.
39 P. Nockemann, K. Binnemans, B. Thijs, T. N. Parac-Vogt, K. Merz, A.-V. Mudring, P. C. Menon, R. N. Rajesh,

G. Cordoyiannis, J. Thoen, J. Leys and C. Glorieux, *J. Phys. Chem. B*, 2009, **113**, 1429.
40 J. P. Perdew, *Phys. Rev. B: Condens. Matter Mater. Phys.*, 1986, **33**, 8822.
41 A. D. Becke, *Phys. Rev. A: At., Mol., Opt. Phys.*, 1988, **38**, 3098.
42 S. H. Vosko, L. Wilk and M. Nusair, *Can. J. Phys.*, 1980, **58**, 1200.
43 University of Karlsruhe and Forschungszentrum Karlsruhe GmbH, TURBOMOLE V6.1 2009, 1989–2007, 25 GmbH, since 2007, available from http://www.turbomole.com.
44 F. Eckert and A. Klamt, COSMOlogic GmbH & Co. KG, Leverkusen, Germany, 2013.
45 M. G. Freire, S. P. M. Ventura, L. M. N. B. F. Santos, I. M. Marrucho and J. A. P. Coutinho, *Fluid Phase Equilib.*, 2008, **268**, 74.
46 M. J. Frisch, G. W. Trucks, H. B. Schlegel, G. E. Scuseria, M. A. Robb, J. R. Cheeseman, G. Scalmani, J. A. Montgomery Jr., T. Vreven, K. N. Kudin, J. C. Burant, J. M. Millam, S. S. Iyengar, J. Tomasi, V. Barone, B. Mennucci, M. Cossi, G. Scalmani, N. Rega, G. A. Petersson, H. Nakatsuji, M. Hada, M. Ehara, K. Toyota, R. Fukuda, J. Hasegawa, M. Ishida, T. Nakajima, Y. Honda, O. Kitao, H. Nakai, M. Klene, X. Li, J. E. Knox, H. P. Hratchian, J. B. Cross, V. Bakken, C. Adamo, J. Jaramillo, R. Gomperts, R. E. Stratmann, O. Yazyev, A. J. Austin, R. Cammi, C. Pomelli, J. W. Ochterski, P. Y. Ayala, K. Morokuma, G. A. Voth, P. Salvador, J. J. Dannenberg, V. G. Zakrzewski, S. Dapprich, A. D. Daniels, M. C. Strain, O. Farkas, D. K. Malick, A. D. Rabuck, K. Raghavachari, J. B. Foresman, J. V. Ortiz, Q. Cui, A. G. Baboul, S. Clifford, J. Cioslowski, B. B. Stefanov, G. Liu, A. Liashenko, P. Piskorz, I. Komaromi, R. L. Martin, D. J. Fox, T. Keith, M. A. Al-Laham, C. Y. Peng, A. Nanayakkara, M. Challacombe, P. M. W. Gill, W. Johnson, W. Chen, M. W. Wong, C. Gonzalez and J. A. Pople, Wallingford, CT, 2004.